An Evaluation of Three Dimensional Diarthrodial Joint Contact Using Penetration Data and the Finite Element Method

W. L. Dunbar, Jr.*, K. Ün, P. S. Donzelli and R. L. Spilker

Department of Biomedical Engineering and the

Scientific Computation Research Center

Rensselaer Polytechnic Institute

Troy NY 12180-3590

*Johnson & Johnson Professional, Inc

Raynham MA 02767-0350

Abstract

We have developed an approximate method for simulating the three-dimensional (3-D) contact of soft biphasic tissues in diarthrodial joints under physiological loading. Input to the method includes: (i) kinematic information describing an *in vitro* joint articulation, measured while the cartilage is deformed under physiological loads, (ii) geometric properties for the relaxed (undeformed) cartilage layers, obtained for the analyses in this study via stereophotogrammetry, and (iii) material parameters for the biphasic constitutive relations used to represent cartilage. Solid models of the relaxed tissue layers are assembled in physiological positions, resulting in a mathematical overlap of the cartilage layers. The overlap distribution is quantified and converted via the biphasic governing equations into applied traction boundary conditions for both the solid and fluid phases for each of the contacting layers. Linear, biphasic, 3-D, finite element analysis is performed using the contact boundary conditions derived for each of the contacting layers. The method is found to produce results consistent with the continuity requirements of biphasic contact. Comparison with results from independent, biphasic contact analyses of axisymmetric problems shows that the method underestimates slightly the contact area, leading to an overestimation of the total traction, but yields a good approximation to elastic stress and solid phase displacement.

Introduction

The soft cartilaginous layers in human diarthrodial joints are capable of supporting high levels of mechanical load over decades, yet degenerative joint diseases still affect millions of people every year. In order to contribute to the understanding of diseases such as osteoarthritis, we must understand the mechanical response of the cartilage layers of both healthy and pathological diarthrodial joints under physiological loading. While experimental investigations are a key component, this understanding is often gained with the aide of mathematical models, such as elastic, biphasic [1] or triphasic [2] theories, used to quantify the mechanics of soft tissues through both analytical and numerical procedures. Much progress has been made in the finite element analysis of soft tissues using the biphasic theory. Various finite element formulations have been developed and implemented [3-10], including nonlinear contributions such as large deformation, a viscoelastic solid phase and contact. While applied to mostly canonical or experimental configurations, all of these components contribute to increasingly representative models of diarthrodial joints that can be used in computer-simulated or computer-aided surgery, prosthetic design, or investigation of degenerative joint diseases. The present study combines a number of contemporary research techniques, and a new approach for approximating joint contact, to form a method of studying the mechanics of contacting tissue layers in diarthrodial joints.

The mechanical behavior of diarthrodial joints is dictated by contact, as forces are transmitted across the joint through the soft tissue layers, but analysis of three-dimensional, multi-phase contact is complicated and computationally demanding. Most contact finite element models have assumed elastic, rigid or viscoelastic material laws [11-15] or been restricted to experimental configurations [16]. These models provide insight into the total stress in the tissues but do not account for the biphasic nature of tissue. An exception is the recent axisymmetric biphasic model of Donzelli et al. [10]. Commercial finite element packages have also been used recently to model biphasic contact, producing reasonable results for axisymmetric cases, although no further information is given about the implementation or computational cost [17, 18]. A major computational challenge remains to derive and perform full 3-D sliding contact of biphasic layers. In an effort to reduce the computational cost, we present a method that approximates soft tissue contact mechanics. The method reduces the problem of two biphasic tissues contacting over an unknown area to two problems, each with prescribed traction

distributions over a fixed area. This replaces the non-linearity of contact analysis with a preprocessing step dependent on the geometry.

From the biphasic continuum theory and contact boundary conditions we derive the necessary equations to compute contact traction distributions from measured tissue geometry and kinematics. This method is implemented in a custom-designed, object oriented preprocessing program to develop the necessary boundary condition input to our biphasic analysis finite element code. Using example problems defined on canonical geometries, we test this method in comparison to analytical and 2-D finite element contact solutions. Our goal is to determine if the method is self-consistent, and how well it compares to biphasic contact analysis. We pose the following specific questions regarding the analysis. (1) Is the required traction continuity enforced when tissues are analyzed independently for a given joint? (2) Does the result compare well with what we observe in contact analysis? (3) Are the results consistent with the kinematic data used to generate the input? (4) Do the shear stresses and strains vanish in accordance with our assumptions of frictionless contact? Specific results will address each of these questions, and demonstrate the validity of the method for physiological joint geometries.

Methods

Linear Biphasic Theory with Contact Boundary Conditions

For this study, we use the linear biphasic theory to model cartilage as a continuum consisting of incompressible solid and incompressible, inviscid fluid phases. The drag created by the movement of the fluid through the solid matrix gives the tissue its viscoelastic properties. In the following equations, the superscripts *s* and *f* refer to the solid and fluid phases, respectively. The biphasic theory [1] imposes a continuity equation for the mixture,

$$\left(\phi^f v_i^f + \phi^s v_i^s\right)_{,i} = 0, \tag{1}$$

where φ^α is the solid or fluid content, v_i^α are solid or fluid velocity components and the comma (,) denotes spatial differentiation; momentum equations for each phase,

$$\sigma_{ij,\,j}^{\alpha} + \Pi_i^{\alpha} = 0, \;\; \alpha = s, f, \tag{2}$$

where Π_i^α is a momentum exchange between phases and σ^α_{ij} are the Cauchy stress tensors; and constitutive equations,

$$\sigma_{ij}^{s} = -\phi^{s} p\delta_{ij} + \sigma_{ij}^{E}, \tag{3}$$

$$\sigma_{ij}^{f} = -\phi^{f} p\delta_{ij}, \tag{4}$$

$$\Pi_{i}^{s} = -\Pi_{i}^{f} = p\phi_{,i}^{s} + K\left(v_{i}^{f} - v_{i}^{s}\right), \tag{5}$$

where p is pressure and K is the diffusive drag coefficient, related to the tissue permeability, κ, through $K = (\phi^{f})^{2} / \kappa$. For a linear elastic solid phase, the elastic part of the solid stress due to deformation is

$$\sigma_{ij}^{E} = C_{ijkl}\varepsilon_{kl}^{s}, \tag{6}$$

where C_{ijkl} is the material property tensor and ε^{s}_{ij} is the infinitesimal elastic strain tensor for the solid phase,

$$\varepsilon_{ij}^{s} = \frac{1}{2}\left(u_{i,j}^{s} + u_{j,i}^{s}\right) \equiv u_{(i,j)}^{s}. \tag{7}$$

Here u^{s}_{i} are the solid phase displacement components and the parentheses in the subscript denote the symmetric part of the deformation tensor.

Boundary and initial conditions on solid displacement, solid or fluid velocity, and solid and fluid traction are required to complete the problem statement. Moreover, there are also boundary conditions between two contacting biphasic bodies, denoted with superscripts A and B [19]. In their frictionless form, these are [20]

$$v_{i}^{sA} n_{i}^{A} + v_{i}^{sB} n_{i}^{B} = 0, \tag{8}$$

$$\left(\phi^{fA} v_{i}^{fA} + \phi^{sA} v_{i}^{sA}\right) n_{i}^{A} + \left(\phi^{fB} v_{i}^{fB} + \phi^{sB} v_{i}^{sB}\right) n_{i}^{B} = 0, \tag{9}$$

$$p^{A} - p^{B} = 0, \tag{10}$$

$$\sigma_{ij}^{E^{A}} n_{i}^{A} n_{j}^{A} - \sigma_{ij}^{E^{B}} n_{i}^{B} n_{j}^{B} = 0, \tag{11}$$

with n_{i} indicating the unit normal components on the contact surface. Physically, Eqs. (8)-(11) represent two kinematic conditions, continuity of normal solid velocity and normal relative flow, and two kinetic conditions, continuity of pressure and normal elastic traction.

Finite Element Formulations of the Biphasic Governing Equations

The governing equations can be manipulated to eliminate fluid velocity, and lead to a mixed velocity-pressure (v-p) finite element formulation. Similar formulations have been used in soil mechanics and biomechanics [3, 7, 21-23]; the version employed here was developed by Almeida [8, 9, 24]. The field variables are solid displacement, and its time derivative, and

pressure. Essential boundary conditions will be specified for these field variables, while total traction and relative flow are the corresponding natural boundary conditions. For the 3-D analyses, we use tetrahedral elements with a quadratic (10-node) interpolation of solid phase displacement and a linear (4-node) interpolation for pressure.

To validate v-p analyses with penetration-based boundary conditions, results will be compared against a mixed-penalty biphasic contact formulation [10] where the contact boundary conditions are included in a weighted residual formation, with the kinetic contact conditions enforced via Lagrange multipliers. This contact formulation is axisymmetric; so all validation cases will be axisymmetric 3-D models.

Approximating Contact Traction from Penetration Data

Our method replaces nonlinear iterative 3-D contact analysis by linear biphasic analysis of each of the contacting tissue layers using a prescribed traction that approximates the contact traction. The following input data is required: (i) joint kinematics, and the resultant force producing those kinematics, at one or more physiological positions; (ii) geometry of the tissue layers in an undeformed state; and (iii) material parameters for the biphasic soft tissues. We use this data and the governing equations in a series of four steps to obtain the approximate traction distribution. First the geometric models of the contacting layers are placed in a physiological position and queried to determine the geometric overlap, or penetration, between the undeformed tissues. Next this vector penetration field is split between the two contacting layers, then scaled to represent a traction. Finally, the traction is divided between the solid and fluid phases of each tissue.

In the first step, the relaxed, undeformed tissue geometries are imported into a solid modeling package (e.g., Parasolid, Shapes [25]), creating mathematical representations of the tissues. Using kinematic data and modeler operations, the tissues are positioned in a known physiological orientation. In this position, the *in-vivo* soft tissues are deformed and in contact. However, in the as-yet-undeformed solid model, the tissue layers will interpenetrate. The penetration at any location on the tissue surfaces can be quantified using the solid modeling software.

The second step is to distribute the total penetration between the contacting tissues. Assume that the traction is being calculated for the analysis of tissue A (Fig. 1); tissue B will be

analyzed in a separate step. In this case, the total penetration vector, $\mathbf{g}^{Tot}$, is measured in a direction normal to the contact surface of tissue A. The local thickness of tissues A and B, h^A and h^B, respectively, are also measured along this normal direction. Let $0 \le \eta \le 1$ be the part of the total penetration that is associated with tissue A. Our analysis is based on the assumption that penetration is locally equal to the total deformation of the layers, so the (solid) displacements of layers A and B are given by:

$$u_i^{s^A} = g_i^A = \eta g_i^{Tot}, \tag{12}$$

$$u_i^{s^B} = g_i^B = (1-\eta) g_i^{Tot}, \tag{13}$$

$$u_i^{s^A} + u_i^{s^B} = u_i^{s^T} = g_i^{Tot}. \tag{14}$$

The parameter η will be evaluated from the continuity of traction on the contact surface, Eq. (11). For convenience, consider an orthogonal tangent-normal coordinate system defined on the loaded face of each layer, and denote the normal and tangential components of a vector with subscripts n, t_1 and t_2, respectively. By construction, the only non-zero component of $\mathbf{g}^A$ is the normal component, g_n^A. In biphasic contact, for constant φ^s, the variation of the pressure is relatively uniform through the thickness, a fact observed both in numerical [26] and semi-analytical studies [27]. Also, the first term in an asymptotic solution for pressure in biphasic contact is not dependent on depth [28]. Thus, it is reasonable to assume that the normal elastic strain is also uniform through the thickness and can be approximated as

$$\varepsilon_{nn}^{s^A} = \frac{\delta h^A}{h^A} = \frac{g_n^A}{h^A}, \tag{15}$$

where δh^A denotes the change in the local thickness of tissue due to deformation (Fig. 1). There are no tangential components in the penetration vector. Although model curvature, or a gradient in the penetration vector with position, could cause in-plane strains ($\varepsilon_{t_1t_1}, \varepsilon_{t_2t_2}, \varepsilon_{t_1t_2}$), we show in Appendix I that the in-plane strains caused by these effects are negligibly small for *in-vivo* joint geometries. Also, for frictionless contact, the shear stresses in tangent-normal coordinates are zero. These assumptions are summarized as

$$\varepsilon_{t_1t_1}^s = \varepsilon_{t_2t_2}^s = \varepsilon_{t_1t_2}^s = 0 \qquad \sigma_{nt_1}^E = \sigma_{nt_2}^E = 0. \tag{16}$$

Returning to the continuity of traction, we can now use the displacement field from the penetration data, Eq. (12), and our simplifying assumptions, Eq. (16), to calculate normal strain, Eq. (15), and then stress. Representing the solid phase of cartilage as transversely isotropic with

the material axis normal to the tissue surface [29, 30], the material property matrix will have the form

$$\begin{Bmatrix} \sigma_{nn} \\ \sigma_{t_1t_1} \\ \sigma_{t_2t_2} \\ \sigma_{t_1t_2} \\ \sigma_{nt_1} \\ \sigma_{nt_2} \end{Bmatrix} = \begin{bmatrix} C_{11} & C_{12} & C_{13} & 0 & 0 & 0 \\ C_{12} & C_{22} & C_{23} & 0 & 0 & 0 \\ C_{13} & C_{23} & C_{33} & 0 & 0 & 0 \\ 0 & 0 & 0 & C_{44} & 0 & 0 \\ 0 & 0 & 0 & 0 & C_{55} & 0 \\ 0 & 0 & 0 & 0 & 0 & C_{66} \end{bmatrix} \begin{Bmatrix} \varepsilon_{nn} \\ \varepsilon_{t_1t_1} \\ \varepsilon_{t_2t_2} \\ \varepsilon_{t_1t_2} \\ \varepsilon_{nt_1} \\ \varepsilon_{nt_2} \end{Bmatrix}, \tag{17}$$

where the terms in the matrix **C** are related to five material parameters and the predominant material direction. Substituting these relations, the first term in Eq. (11) becomes

$$\sigma_{ij}^{E^A} n_i n_j = C_{ijkl}^A \varepsilon_{kl}^{s^A} n_i n_j \approx C_{11}^A \varepsilon_{nn}^{s^A} = C_{11}^A \frac{\eta g_n^{Tot}}{h^A}. \tag{18}$$

The same calculations are performed for tissue B, using Eq. (13), and yield the following expression for the second term in Eq. (11):

$$\sigma_{ij}^{E^B} n_i n_j = C_{ijkl}^B \varepsilon_{kl}^{s^B} n_i n_j \approx C_{11}^B \varepsilon_{nn}^{s^B} = C_{11}^B \frac{(1-\eta) g_n^{Tot}}{h^B}. \tag{19}$$

Substituting Eqs. (18) and (19) into Eq. (11) and solving for η gives

$$\eta = \frac{1}{\left(1 + \frac{C_{11}^A h^B}{C_{11}^B h^A}\right)}, \tag{20}$$

which indicates that the penetration is shared between the layers on the basis of the local modulus and thickness of the contacting tissues (both of which may vary *in-vivo*). Note that for an isotropic solid phase,

$$C_{11} = H_A = \left(2\mu^s + \lambda^s\right), \tag{21}$$

where H_A is the aggregate modulus and μ^s and λ^s are the Lamé parameters of the solid phase.

The third step is to calculate the total normal traction acting on a tissue layer. Here we make use of an observation originating from the axisymmetric 2-D biphasic contact code and assume the distribution of total normal traction over the contact area to be linearly related to the normal strain. Because the tissue is biphasic, this implies that the pressure at the contact surface is also linearly related to the normal strain. This leads to the expression

$$\mathbf{t}^{Tot} = \gamma^A \frac{\mathbf{g}^A}{h^A}, \tag{22}$$

where $\mathbf{t}^{Tot}$ is the vector of total traction and γ^A is a proportionality constant. Equation (22) requires that the total traction vector be parallel to the penetration vector, and therefore normal to the contact surface, consistent with the assumption of frictionless contact. Thus for any component of the resultant force vector **F** applied on the joint, we can write

$$\int_{\Gamma^c} t_i^{Tot}\, d\Gamma^c = \gamma^A \int_{\Gamma^c} \frac{g_i^A}{h^A}\, d\Gamma^c = F_i \tag{23}$$

We calculate γ^A by requiring that the magnitude of the resultant force produced by the total traction be equal to the force applied to the joint, |**F**|, This gives

$$\gamma^A = \frac{|\mathbf{F}|}{\sqrt{\sum_{i=1}^{3} \left(\int_{\Gamma^c} \frac{g_i^{Tot}}{h^A}\, d\Gamma^c \right)^2}} \tag{24}$$

In the final step, the applied load must be partitioned between the solid and fluid phases [19], and this partitioning cannot be determined experimentally. A load sharing parameter, $\phi^s \le \phi^* \le 1$, is defined over the contact surface as the percentage of the total traction that is carried by the solid phase. A φ^* value of 1 indicates that the load is fully supported by the solid phase, and a value of φ^s that the load is supported by the pressure, in which case only a fraction equal to φ^s is carried by the solid phase (Eq. (3)). The normal components of solid and fluid traction can be written as

$$t_i^s n_i = \sigma_{ij}^s n_i n_j = \phi^* \sigma_{ij}^{Tot} n_i n_j \tag{25}$$

$$t_i^f n_i = \sigma_{ij}^f n_i n_j = \left(1 - \phi^*\right) \sigma_{ij}^{Tot} n_i n_j \tag{26}$$

Using the constitutive relations, Eqs. (3) and (4), pressure can be related to the normal components of total and elastic traction,

$$p = \sigma_{ij}^E n_i n_j - \sigma_{ij}^{Tot} n_i n_j . \tag{27}$$

Substituting Eqs. (27) and (3) into Eq. (25) gives the following expression for the partitioning factor,

$$\phi^* = \frac{\sigma_{ij}^s n_i n_j}{\sigma_{ij}^{Tot} n_i n_j} = \phi^s + \phi^f \left(\frac{\sigma_{ij}^E n_i n_j}{\sigma_{ij}^{Tot} n_i n_j} \right) \tag{28}$$

Incorporating expressions for the elastic traction, Eq. (18), and the total traction, Eq.(22), gives

$$\phi^* = \phi^s + \phi^f \left(\frac{C_{11}}{\gamma} \right) \tag{29}$$

The objective is to apply essential or natural boundary conditions to enforce this partitioning of the traction. For the v-p formulation, this is achieved by specifying total traction, calculated from Eq. (22), as a natural boundary condition, thus contributing to the applied load vector in the biphasic finite element equations. Pressure is an essential condition on the same boundary, leading to specified nodal values that are calculated using Eq. (27). Unlike contact analysis, which requires nonlinear iteration to resolve the unknown contact area, this penetration-based method generates applied traction loads for each layer in the preprocessing stage. After preprocessing, the layers can be analyzed independently using 3-D biphasic analysis.

As commonly done in finite element analysis, shape functions and the finite element mesh are utilized to define the spatial distribution of overlap required to evaluate the integrals in Eq. (24) numerically. Using γ, the distribution of total traction is determined from Eq. (22) and φ^* is calculated using Eq. (29), from which the pressure can be calculated. Knowing total traction and pressure, the essential and natural boundary conditions can be specified in the zone of contact.

It should be noted that the partitioning factor in our method is constant in time, whereas the theoretical partitioning factor for contact of biphasic materials is time-dependent (i.e., equal to φ^s at $t=0^+$ and approaching unity for large time). However, we are not interested in analyses at either one of these extremes. The time $t=0^+$, while of potential mathematical interest, plays no role in our analyses, which are intended to be performed for times of the order of seconds, and large times are unrealistic for human motion. In addition, the contact area and penetration distribution over that area do not change with time. We will extend our method in the future in order to use more complete kinematics data to vary the partitioning factor, contact area, and penetration distribution. In that case, the analysis can be applied to longer time ranges, and to the more realistic moving contact problem.

Examples

Problem Definition

We validate the penetration method for the short-time response of two canonical problems whose geometry, Fig. 2, and properties resemble the glenohumeral joint in the human

shoulder. The lower and upper tissues in each case are referred to as layers A and B, respectively. The radii of curvature of the articular surface and the bone surface are denoted by R_{Ac} and R_{Ab}, respectively, for the lower layer, and R_{Bc} and R_{Bb} for the upper layer. The thickness of layers A and B at the axis of rotation are t_A and t_B. For case CT the thickness is constant, and for case VT the thickness varies with radial position. The geometric parameter values for each case are also shown in Fig. 2. Layers of rigid, impermeable bone support the cartilage layers and an axially-directed force is applied to the upper layer through the bone. The first geometric model consists of two tissues having the same thickness, but different radii of curvature; in the second model, tissue A is 50% thicker than tissue B. Note that tissue thickness varies with position from the axis of rotation. We quantify the congruency of contact as follows:

$$\frac{1}{R_{Bc}} - \frac{1}{R_{Ac}} = \frac{1}{congruency} \tag{30}$$

The first example (CT) is more congruent than the second (VT).

All tissue layers have a Young's modulus, E = 556 kPa, Poisson's ratio, $\nu = 0.05$, permeability, $\kappa = 1.7\times10^{-15}$ m^4/Ns and solid content, $\varphi^s = 0.25$. To understand the influence of variable material properties on the preprocessing calculations, the same cases were also run with Young's modulus halved in layer B. A force of 75 N is applied to the rigid bone of the upper layer over a linear 0.1 s ramp, then held constant for an additional 0.1 s.

Each configuration is analyzed first using the 2-D axisymmetric biphasic contact finite element [10], from which the displacement of the upper rigid body at t=0.2s is computed. This displacement value is then applied within the solid modeler to the upper layer of the 3-D solid model, allowing it to rigidly penetrate the lower layer of the model. Preprocessing starts by quantifying this penetration. After obtaining the total traction and the partitioning factor, φ^*, as described earlier, the corresponding 3-D analysis is run using a time step of $\Delta t=0.01$s. Results are compared with those obtained from the 2-D biphasic contact analyses.

Results

Results obtained for the normal component of elastic traction and the pressure in layers A and B for cases CT and VT at t = 0.1 s are shown in Figs. 3a, where the moduli of layer A and B are identical, and 3b, where the modulus of layer B is half that of layer A. These results confirm that the penetration-based method satisfies traction and pressure continuity (see Eqs. (10) and (11)) on the contacting surface. While not shown, similar results are obtained at other times. The

maximum deviation between corresponding values from layers A and B is approximately 1% for the pressure.

Elastic traction distributions at the end of the ramp time for layer A in cases CT and VT compare well with values from the axisymmetric contact analysis (Fig. 4.). As is evident in the figure, the contact radius predicted by the penetration method can be significantly less than that found by the contact analysis, depending on the congruity of the contacting layers (20% less for case CT compared with 10% for case VT). As a result, solid traction, total traction (see Fig. 5), and pressure are generally overestimated. While not explicitly shown here, note that our method assumes a load sharing parameter, φ^*, that is constant within the contact region, while the value calculated by the biphasic contact analysis decreases toward the edge of contact. For example, computed values of φ^* at the center of the 3-D penetration model are about 15% less for case CT and 10% less for case VT, compared with the axisymmetric biphasic contact solution.

Figure 6 compares the normal displacement predicted by the 3-D penetration analysis and axisymmetric contact analysis along the contact surfaces for layers A and B at the end of the ramp time. While only compressive loads are applied, note that that the penetration method captures the positive displacements at the edge of contact.

While not explicitly shown here, we note that the surface shear stresses are negligibly small compared with the normal traction components. Likewise, shear strains on the contact surface are typically < 5% of the corresponding normal strains.

Discussion

In this study we developed a penetration-based method to approximate three-dimensional biphasic contact and evaluated the method for axisymmetric contact problems for which an independent contact method and solution are available. Validation requires acceptable approximation of the contact continuity conditions and the subsequently calculated field variables, such as tissue deformation, stress and strain. Our analyses show that the penetration method provides a good approximation to the continuity requirements of contact. This remains true if the contacting layers have non-uniform thickness and different material properties, because the derived splitting parameter for penetration, η, accounts for variations in these problem parameters.

As predicted by the 2-D axisymmetric biphasic contact analysis, bulging of the convex layer produces a larger contact area, and this effect depends on joint congruency. Our method cannot capture this effect, and the error in estimating the contact area is larger for more congruent geometries. Due to this underestimated contact area, the total normal traction is overestimated in the penetration method compared to contact analysis, since total force is prescribed. The error in the contact area also leads to the underestimation of the integral in the denominator of Eq.(24). As a result, the proportionality constant that scales penetration to traction, γ, is higher, and hence, in view of Eq.(29), φ^* is smaller.

Normal elastic tractions from the penetration-based analysis compared well with the biphasic contact analysis. According to Eq.(18), elastic traction depends only on the normal strain value calculated from the penetration data and the aggregate modulus. Using Eq.(28), the normal elastic traction can be expressed as a function of total traction and φ^*,

$$\sigma_{ij}^{E} n_i n_j = \frac{(\phi^* - \phi^s)}{\phi^s} \sigma_{ij}^{T} n_i n_j . \tag{31}$$

According to Eq.(31), if the elastic traction is estimated well, the effect of overestimated total normal traction should be more or less canceled by the underestimated partitioning factor φ^*. This is the case for the error that we make in total normal traction and φ^* calculations, since our examples demonstrate that the estimatation of normal elastic traction is accurate. The accuracy of the normal elastic traction is of great importance since it demonstrates the potential of the penetration method to capture the essential phenomena of contact.

The displacement values from the 3-D penetration-based analysis compare relatively well with the biphasic contact analysis, the deviation mainly caused by the bulging effect, which cannot be exactly captured by the penetration method. Recall that our method assumes that the penetration approximates the normal deformation of the contact surface, from which the applied traction is eventually derived. The actual deformation is subsequently calculated in the 3-D biphasic analysis. The displacement that the analysis returns, in general, is close to the penetration data; this confirms the validity of the assumption that the penetration is equivalent to the normal deformation. Note that the calculation of the normal strain in the preprocessing step, and the calculation of η, which splits the penetration data between the layers, are also verified with these results.

Although not explicitly shown in this paper, we note that the shear strains and stresses are found to be much smaller than the normal stresses and strains, consistent with frictionless contact and the assumptions that we made in the derivation of the normal elastic traction.

Quantities such as the maximum principal stress and the maximum shear stress, and their variations throughout the tissue layers, are significant when assessing the biomechanical aspects of joint mechanics. In the current work we focused mainly on the capability of the penetration method to simulate the biphasic contact conditions. Since we are using a validated 3-D finite element formulation [8] it is clear that a good approximation of the contact traction will lead to an accurate volumetric solution. Three dimensional stress and strain responses for the axisymmetric problems presented here agree with the corresponding 2-D contact code, and we are presently performing parametric studies that look at variations in stress to assess the possibility of failure in physiological shoulder models.

The penetration-based method has been developed as an interim method, but it also has the long range potential to provide good approximations while significantly reducing the computational resources needed to analyze 3-D contact. Our experience in the present study showed that, even compared to 2-D axisymmetric contact analysis, the penetration method requires significantly less CPU time. The difference will be much more significant when compared with 3-D contact analysis. In these analyses, our 3-D meshes have approximately 5000-6000 elements that take a CPU time of 30 minutes (including 20 time steps taken) on a SUN UltraSparc 60 workstation.

Our method reduces the computational complexity of three-dimensional contact analysis by replacing the nonlinear iterative process involving multiple contacting bodies with individual 3-D analyses of the contacting bodies under pre-calculated surface traction. The method has been validated for canonical joint problems that are axisymmetric and can therefore be analyzed using both 2-D axisymmetric biphasic contact methods and our 3-D penetration-based method. Although our method is a linear (non iterative) approximation to the true contact problem, the results show good agreement with biphasic contact analysis and give us confidence to carry forward with physiological problems involving complex geometries. There are other improvements to the method that are under development. They include extension to smoothly traveling loads typical of joint motion, in contrast to the discrete positioning of joints used here, and incorporation of tissue nonlinearities. We are also continuing the development of 3-D

biphasic contact, which will provide the true standard against which we can evaluate the penetration-based method.

Acknowledgment

This work was supported by the National Science Foundation (ECS-9024235), the National Institutes of Health (R01 AR42850) and the Surdna Foundation.

Appendix

Typical tissue layers in the musculoskeletal system have curved faces. Assigning a displacement at each point that is normal to the surface, as done in the penetration method, will cause a corresponding tangential displacement. Here we demonstrate that the associated tangential strains are small compared to the normal strain and can be neglected in the elastic traction calculation in the pre-processing step. In the case of a flat surface the analysis is similar.

Consider a distribution of penetration vectors that is normal to a surface of curvature R, Fig A1. For simplicity let R be constant. Considering a small angle, denoted as $\delta\theta$, a line segment of length d takes the length d' after the penetration field **g** deforms the surface. It is clear that $d=R\delta\theta$ and the cosine law gives

$$d'^2 = (R-g)^2 + (R-g-\delta g)^2 - 2(R-g)(R-g-\delta g)\cos(\delta\theta). \tag{A.1}$$

For a small angle $\delta\theta$

$$1-\cos(\delta\theta) \approx \frac{(\delta\theta)^2}{2}. \tag{A.2}$$

Using this equation and neglecting higher order terms, Eq. (A.1) can be rearranged to the following form:

$$d' \approx R\delta\theta\sqrt{(1-\frac{g}{R})^2 - (1-\frac{g}{R})\delta g + \frac{1}{R^2}(\frac{\delta g}{\delta\theta})^2}\ . \tag{A.3}$$

The tangential strain corresponding to this length change is

$$\varepsilon = \frac{d'-d}{d}. \tag{A.4}$$

Substituting Eq. (A.3) into Eq. (A.4) and arranging terms gives

$$\varepsilon = \frac{R\delta\theta\sqrt{(1-\frac{g}{R})^2 - (1-\frac{g}{R})\delta g + \frac{1}{R^2}(\frac{\delta g}{\delta\theta})^2} - R\delta\theta}{R\delta\theta}. \tag{A.5}$$

The second term in the square root is of lower order and is neglected. The third term in the square root indicates (the square of) the change of penetration value per unit distance covered on the curved surface. For a paraboloidal penetration distribution with maximum value g_{max} over a circle of radius R_o, the maximum value that this quantity can take will be equal to $2g_{max}/R_o$. In our example problems, g_{max} and R_o are O(0.1mm) and O(10mm), respectively, so that this term is O(0.0001mm) and can be neglected compared to the first term, which is O(1). With these considerations, Eq. (A.5) simplifies to

$$\varepsilon \approx -\frac{g}{R}. \tag{A.6}$$

Recall that in the analysis the magnitude of the normal strain is given as

$$\varepsilon_n = \frac{g}{h}, \tag{A.7}$$

where h is the local thickness of the tissue. As a result, we can say

$$\frac{\varepsilon}{\varepsilon_n} = O(\frac{h}{R}). \tag{A.8}$$

For a typical glenoid cartilage this quantity is around O(0.1). For a typical humeral head cartilage and for our example geometries it is even smaller.

The result for a flat surface can be derived from Eq.(A.5) by letting $R \to \infty$. In this case, the term δg becomes significant while other terms vanish. Again, using a paraboloidal distribution it can be shown that

$$\frac{\varepsilon}{\varepsilon_n} = O(\frac{hg_{max}}{R_0^2}), \tag{A.9}$$

which is O(0.001) for our example problems. For physiological problems the ratio can have a higher order but is still negligible. The contribution of these in-plane strains to normal elastic traction on the surface is further diminished since they multiply smaller material properties for both isotropic and transversely isotropic material properties of typical soft tissue.

Bibliography

[1] Mow, V.C., Kuei, S.C., Lai, W.M., and Armstrong, C.G., 1980, "Biphasic creep and stress relaxation of articular cartilage in compression: theory and experiments", *Journal of Biomechanical Engineering*, **102,** pp. 73-84.

[2] Lai, W.M., Hou, J.S., and Mow, V.C., 1991, "A triphasic theory for the swelling and deformational behaviors of articular cartilage", *Journal of Biomechanical Engineering*, **113,** pp. 245-258.

[3] Oomens, C.W.J., Van Campen, D.H., and Grootenboer, H.J., 1987, "A mixture approach to the mechanics of skin", *Journal of Biomechanics*, **20,** pp. 877-885.

[4] Suh, J.-K., Spilker, R.L., and Holmes, M.H., 1991, "A penalty finite element analysis for nonlinear mechanics of biphasic hydrated soft tissue under large deformation", *International Journal for Numerical Methods in Engineering*, **32,** pp. 1411-1439.

[5] Spilker, R.L. and Maxian, T.A., 1990, "A mixed-penalty finite element formulation of the linear biphasic theory for soft tissues", *International Journal for Numerical Methods in Engineering*, **30,** pp. 1063-1082.

[6] Vermilyea, M.E. and Spilker, R.L., 1992, "A hybrid finite element formulation of the linear biphasic equations for soft hydrated tissues", *International Journal for Numerical Methods in Engineering*, **33,** pp. 567-594.

[7] Wayne, J.S., Woo, S.L.-Y., and Kwan, M.K., 1991, "Application of the u-P finite element method to the study of articular cartilage", *Journal of Biomechanical Engineering*, **113,** pp. 397-403.

[8] Almeida, E.S. and Spilker, R.L., 1997, "Mixed and penalty finite element models for the nonlinear behavior of biphasic soft tissues in finite deformation: Part I - Alternate formulations", *Computer Methods in Biomechanics and Biomedical Engineering*, **1,** pp. 25-46.

[9] Almeida, E.S. and Spilker, R.L., 1998, "Mixed and penalty finite element models for the nonlinear behavior of biphasic soft tissues in finite deformation: Part II - Nonlinear examples", *Computer Methods in Biomechanics and Biomedical Engineering*, **1,** pp. 151-170.

[10] Donzelli, P.S. and Spilker, R.L., 1998, "A contact finite element formulation for biological soft hydrated tissues", *Computer Methods in Applied Mechanics and Engineering*, **153,** pp. 63-79.

[11] Schreppers, G.J.M.A., Sauren, A.A.H.J., and Huson, A., 1990, "A numerical model of the load transmission in the tibio-femoral contact area", *Journal of Engineering in Medicine*, **204,** pp. 53-59.

[12] Tissakht, M. and Ahmed, A.M., 1990, "Effect of tibial axial rotation on knee meniscal stress: a finite element study", in *Transactions of the 36th Annual Meeting of the Orthopaedic Research Society*, T.M. Wright ed. ORS, Park Ridge, IL, 15, pp. 243

[13] Tissakht, M. and Ahmed, A.M., 1992, "Parametric study using different elastic and poroelastic axisymmetric models of the femur-meniscus-tibia unit", in *Advances in Bionegineering, Winter Annual Meeting of ASME*, M.W. Bidez ed. ASME, New York, BED-Vol. 22, pp. 241-244

[14] Tissakht, M., Marchand, F., and Ahmed, A.M., 1991, "Non-linear finite element analysis of the knee menisci: a composite fiber-reinforced model", in *Transactions, 37th Orthopaedic Research Society Meeting*, 16, pp. 294

[15] Yu, H. and Stone, J.S., 1998, "Viscoelastic Finite Element Contact Analysis of Articular Joints", in *Proceedings of the 1998 Bioengineering Conference*, A.P. Yoganathan ed. ASME, BED-39, pp. 217-218

[16] Hale, J.E., Rudert, M.J., and Brown, T.D., 1993, "Indentation assessment of biphasic mechanical property deficits in size-dependent osteochondral defect repair", *Journal of Biomechanics*, **26,** pp. 1319-1325.

[17] Wu, J.Z., Herzog, W., and Epstein, M., 1998, "Evaluation of the finite element software ABAQUS for biomechanical modelling of biphasic tissues", *Journal of Biomechanics*, **31,** pp. 165-169.

[18] Nilsson, M.C., Davy, D.T., and Mansour, J.M., 1997, "Beneficial mechanical effects of femoral hypertrophy", in *Transactions of the 43rd Annual Meeting of the Orthopaedic Research Society*, L.J. Sandell ed. ORS, Palatine, IL, 22, pp. 828

[19] Hou, J.S., Holmes, M.H., Lai, W.M., and Mow, V.C., 1989, “Boundary conditions at the cartilage-synovial fluid interface for joint lubrication and theoretical verifications”, *Journal of Biomechanical Engineering*, **111,** pp. 78-87.

[20] Ateshian, G.A., 1994, “A theoretical model for boundary friction in articular cartilage”, *Annals of Biomedical Engineering*, **22,Suppl 1,** pp. 63.

[21] Simon, B.R., Wu, J.S.S., Zienkiewicz, O.C., and Paul, D.K., 1986, “Evaluation of U-W and U-P finite element methods for the dynamic response of saturated porous media using one-dimensional models”, *International Journal for Numerical and Analytical Methods in Geomechanics*, **10,** pp. 483-499.

[22] Oomens, C.W.J. and Van Campen, D.H., 1987, “In vitro compression of a soft tissue layer on a rigid foundation”, *Journal of Biomechanics*, **20,** pp. 923-935.

[23] Mish, K.D., Herrmann, L.R., and Muraleetharan, K., 1992, “A comparison of Biot formulation finite element models for two- and three-dimensional transient soil problems”, in *Symposium on Computational Mechanics of Porous Materials and their Thermal Decomposition*, N.J. Salamon and R.M. Sullivan eds., ASME, New York, AMD 136, pp. 69-79

[24] Almeida, E.S. and Spilker, R.L., 1998, “Finite element formulations for hyperelastic transversely isotropic biphasic soft tissues”, *Computer Methods in Applied Mechanics and Engineering*, **151,** pp. 513-538.

[25] Parasolid, 1994, *Version 6 KI Programming Reference Manual*, Electronic Data Systems Corporation, Maryland Heights, MO

[26] Donzelli, P.S., 1995, “A Mixed-Penalty Contact Finite Element Formulation for Biphasic Soft Tissues”, Ph.D. thesis, Rensselaer Polytechnic Institute, Troy, NY

[27] Kelkar, R. and Ateshian, G.A., 1999, “Contact creep of biphasic cartilage layers”, *Journal of Biomechanical Engineering*, **66,** pp. 137-145.

[28] Ateshian, G.A., Lai, W.M., Zhu, W.B., and Mow, V.C., 1994, “An asymptotic solution for the contact of two biphasic cartilage layers”, *Journal of Biomechanics*, **27,** pp. 1347-1360.

[29] Cohen, B., Gardner, T.R., and Ateshian, G.A., 1993, “The influence of transverse isotropy on cartilage indentation behavior -- A study of the human humeral head”, in *Transactions of the 39th Annual Meeting of the Orthopaedic Research Society*, ORS, Park Ridge, IL, 18, pp. 185

[30] Donzelli, P.S., Spilker, R.L., Ateshian, G.A., and Mow, V.C., 1999, "Contact analysis of biphasic transversely isotropic cartilage layers and correlations with tissue failure", *Journal of Biomechanics*, **32,** pp. 1037-1047.

Figure Captions

Figure 1: Definition of penetration quantities for the analysis of tissue A. The total penetration measured along the surface normal of tissue A is denoted as g^{Tot}. To analyze A, the thicknesses of both tissues, denoted as h^A and h^B, are also measured along this surface normal.

Figure 2: Problem definition and geometry for the 2-D biphasic contact and 3-D penetration-based analyses. Cartilage layers (dark gray) are attached to rigid bone (light gray). A force is applied along the axis of symmetry. The centerline thickness of layer A and layer B, and radii of curvature are defined. The geometry shown is for case VT. The corresponding geometric parameters for cases CT and VT are given in millimeters in the table.

Figure 3: Comparison of normal elastic traction and pressure on layers A and B obtained from penetration and contact analysis for both case CT and VT plotted as a function of the distance (radius) from the axis at t=0.1 s. Contacting pairs have the same Young's moduli (3a) or layer B has half the Young's modulus of layer A (3b).

Figure 4: Normal elastic traction on layer A of case CT obtained from penetration and contact analysis plotted as a function of the distance (radius) from the axis at t=0.1 s. at t=0.1 s.

Figure 5: Total normal traction on layer A of case VT obtained from penetration and contact analysis plotted as a function of the distance (radius) from the axis at t=0.1 s.

Figure 6: Axial displacement on layers A and B of case CT obtained from penetration and contact analysis plotted as a function of the distance (radius) from the axis at t=0.1 s.

Figure A1: The penetration distribution assigned to a curved surface, where g denotes the varying penetration field and R is the radius of curvature. Line segment of length d takes the length d' after penetration is applied.

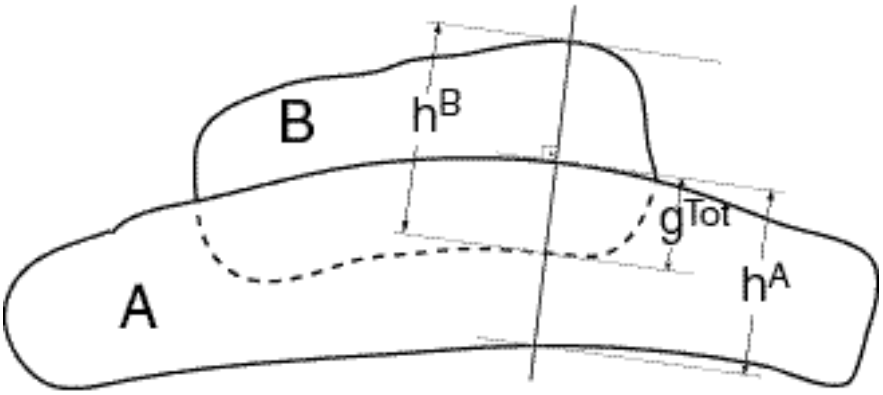

Figure 1

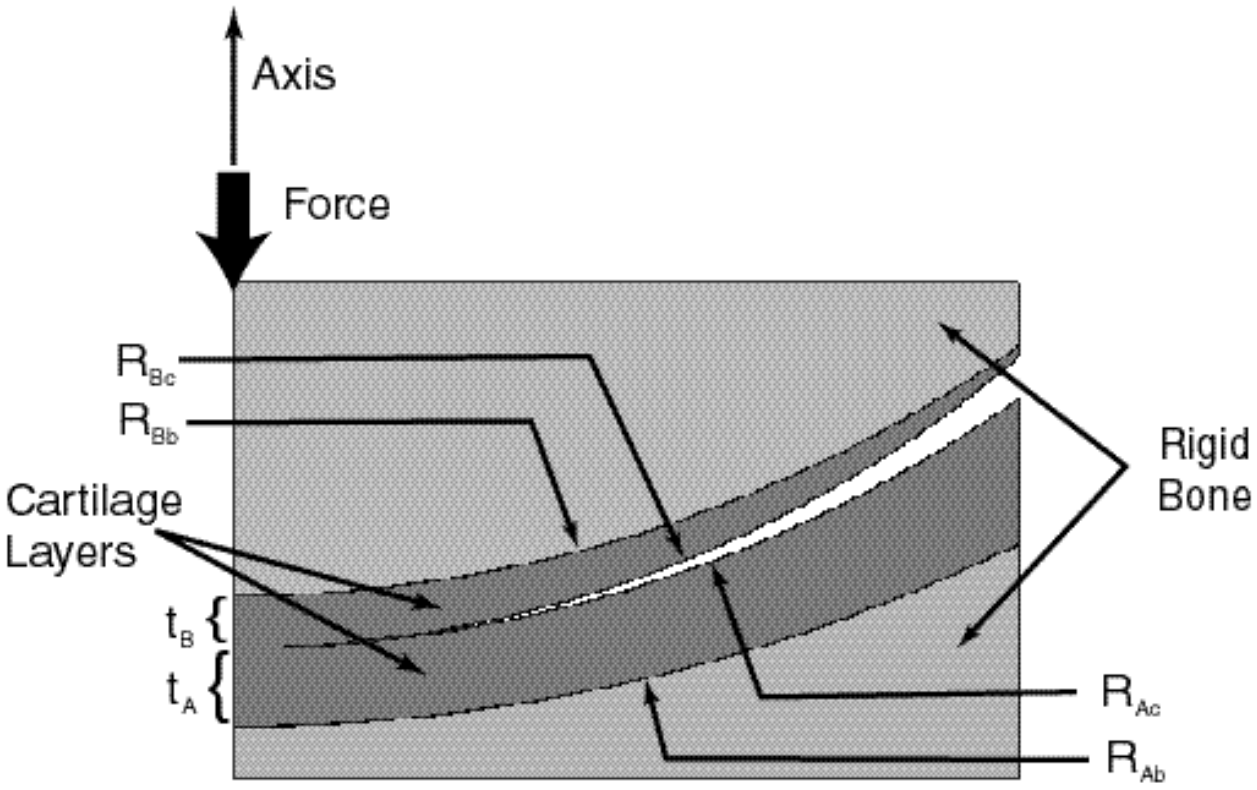

Case	R_{Ac}	R_{Ab}	R_{Bc}	R_{Bb}	t_A	t_B	congruency
CT	26	26	25	25	1.0	1.0	650
VT	26	34	23	26	1.5	1.0	200

Figure 2

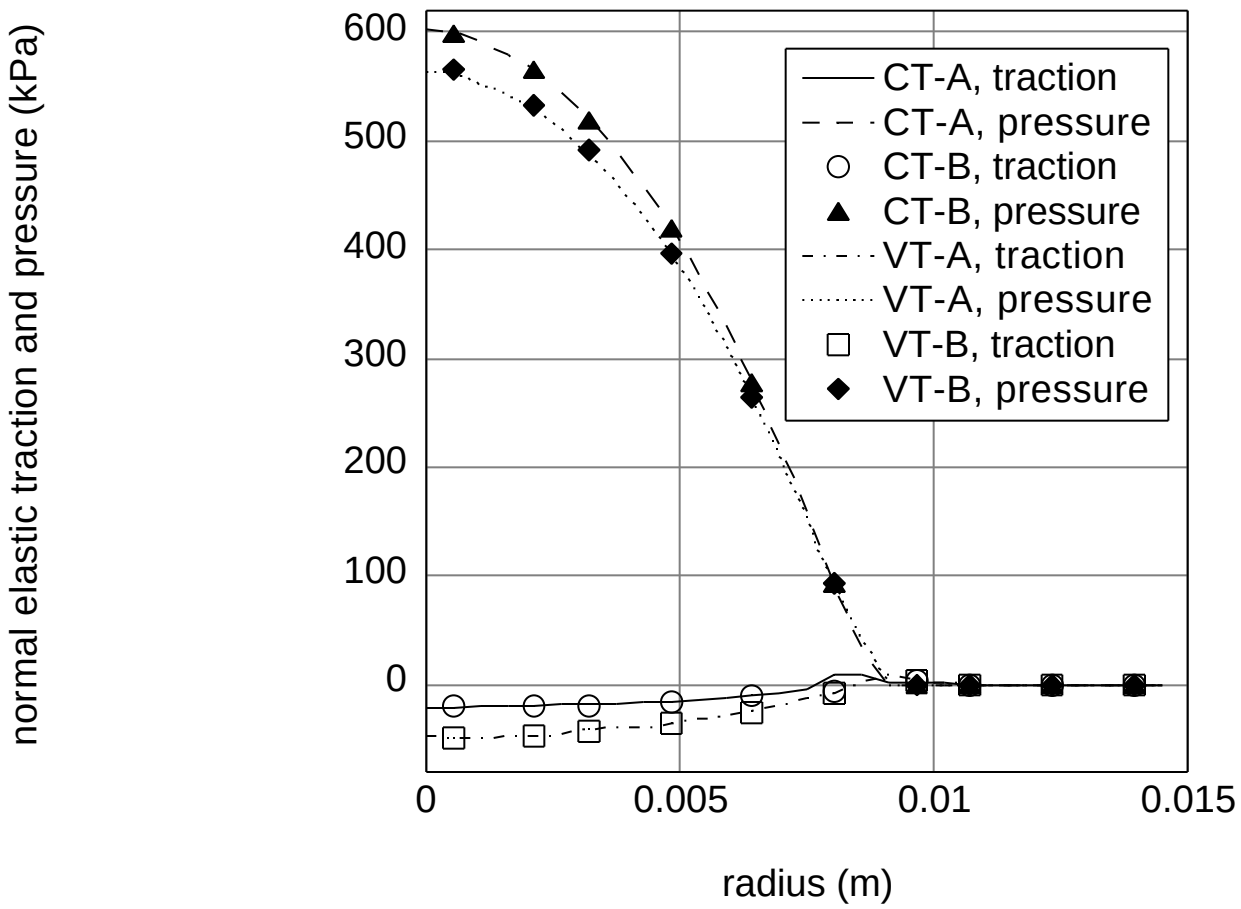

Figure 3a Moduli of tissues A and B are the same.

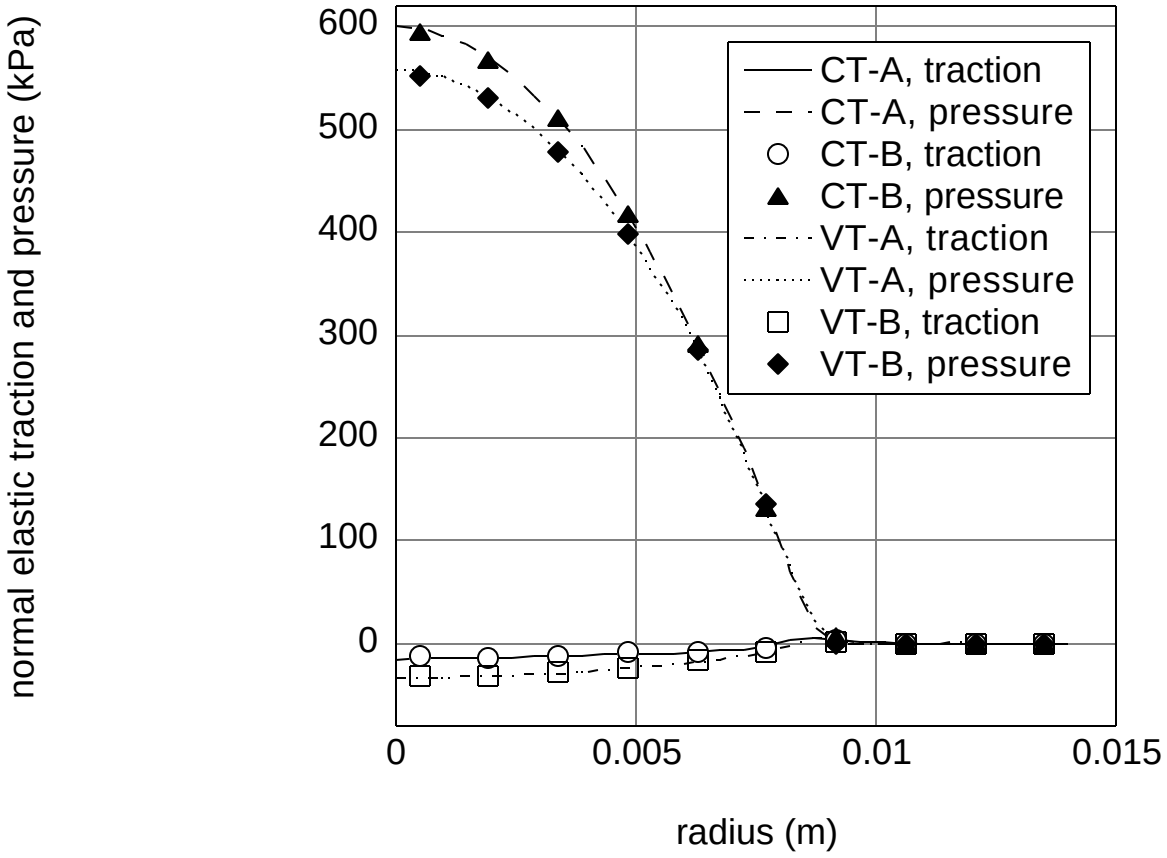

Figure 3b Modulus of tissue B is half the modulus of tissue A.

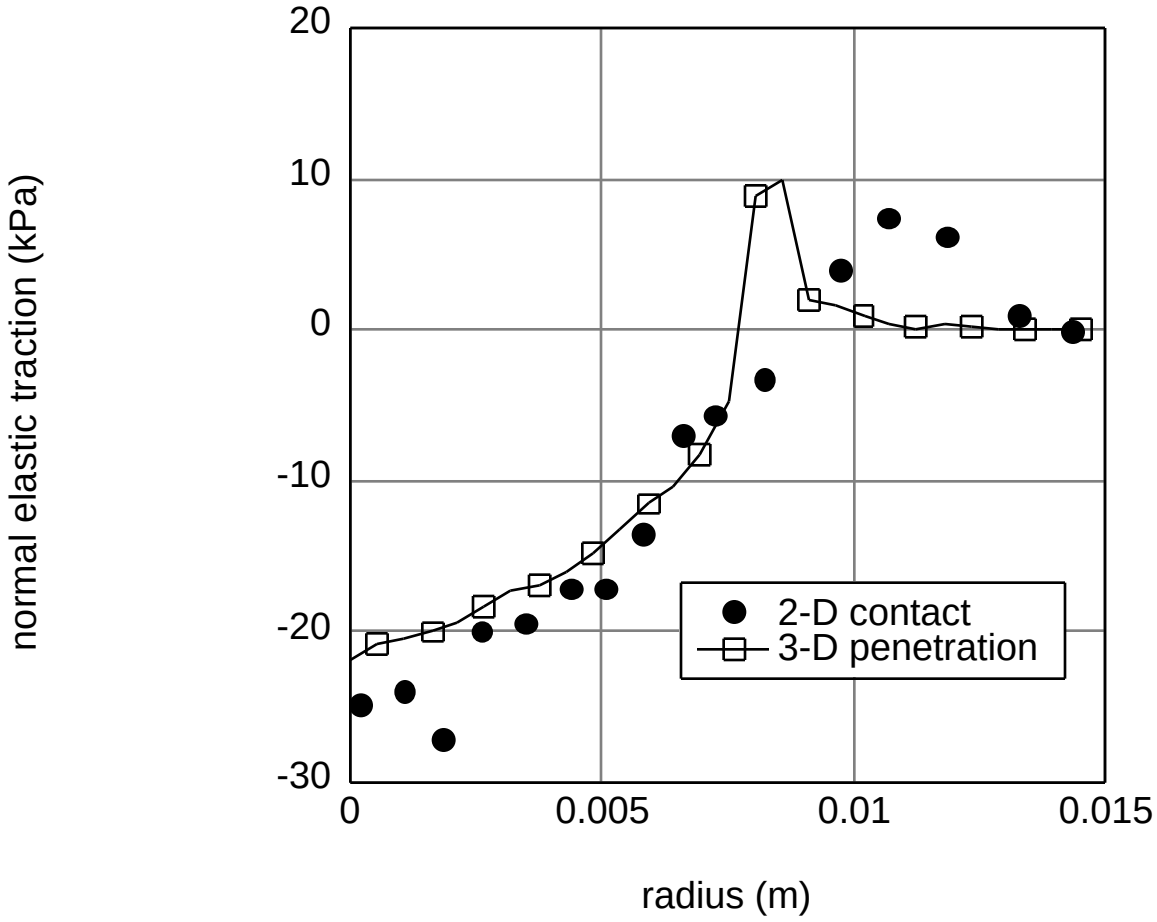
20
10
0
-10
-20
-30
0
0.005
0.01
0.015
normal elastic traction (kPa)
radius (m)
2-D contact
3-D penetration

Figure 4

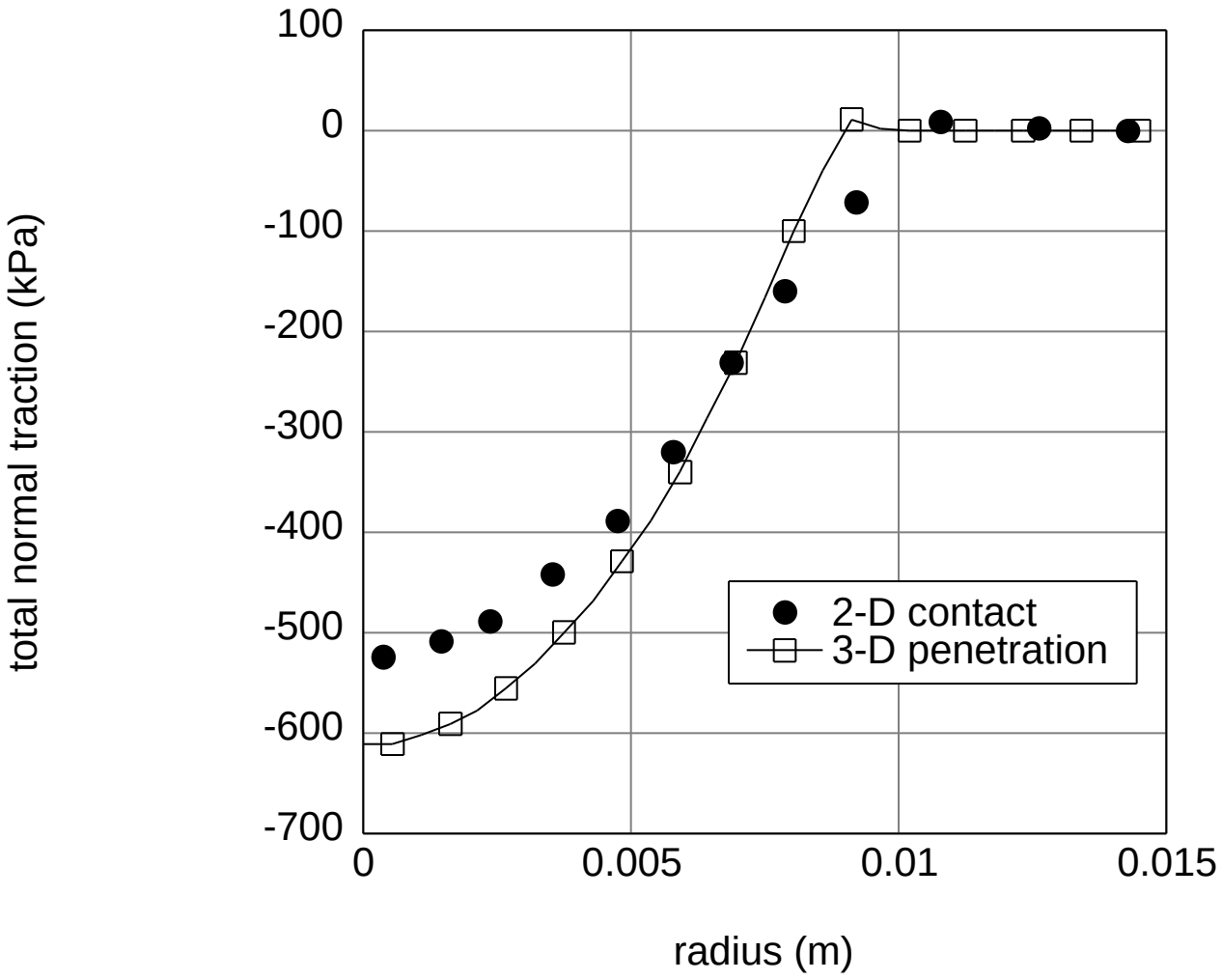
total normal traction (kPa)
100
0
-100
-200
-300
-400
-500
-600
-700
0
0.005
0.01
0.015
radius (m)
2-D contact
3-D penetration

Figure 5

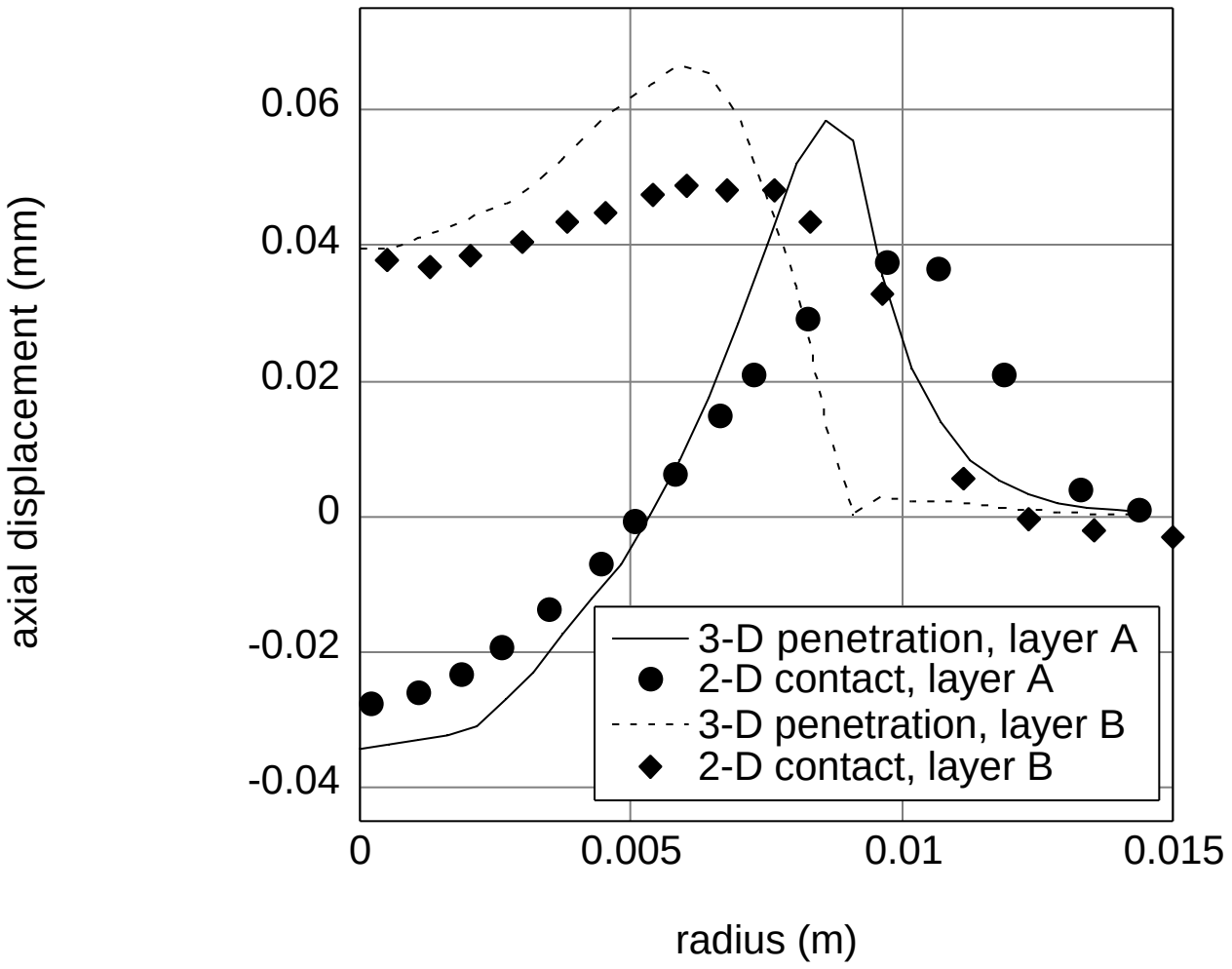
axial displacement (mm)
0.06
0.04
0.02
0
-0.02
-0.04
0
0.005
0.01
0.015
radius (m)
3-D penetration, layer A
2-D contact, layer A
3-D penetration, layer B
2-D contact, layer B

Figure 6

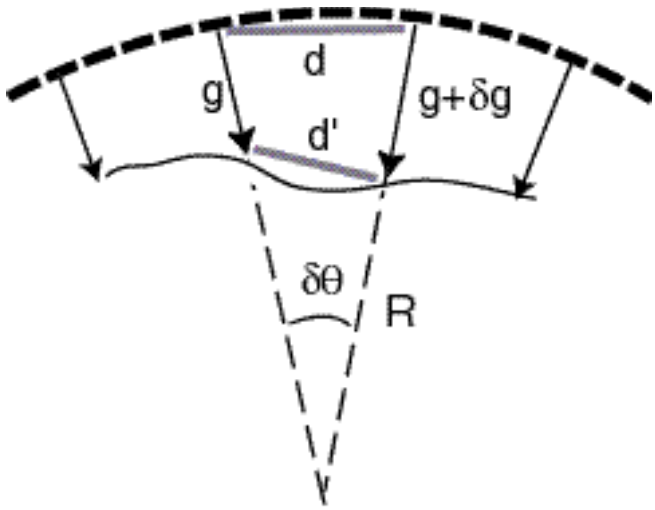

Figure A1